A Study of the Presence of Sahara Dust in the South Texas Sand Sheet, in Kenedy County, Texas

By

Kristie S. Linstead

A thesis submitted in partial fulfillment

of the requirements for the degree of

MASTER OF SCIENCE

in

Geosciences

Middle Tennessee State University

May 2022

ACKNOWLEDGEMENTS

I would like to thank my advisor, Dr. Henrique Momm, for helping me fulfill this degree, as I will be the first in my family to graduate with a master's degree. I would like to thank Dr. Racha ElKadiri and Dr. Clay Harris for reading my countless drafts and helping me make my thoughts much more readable. A special thanks goes to Dr. Warner Cribb for helping me comprehend and graph my results. I am incredibly grateful for Andrew Gibson, Hannah Jones, and Brie Paladino your help and friendship, which helped me get through the last two years. Finally, I need to thank my parents for their support and encouragement while pursuing my degree, and, of course, my son, Kaeden, as I did this for you.

ABSTRACT

The South Texas Sand Sheet (STSS), located within Kenedy County, Texas, is a semi-stabilized dune system. Holocene and Pleistocene quartzose sands define the unique geologic substrate of the STSS. Dune migration and burial of vegetation have led to the development of interbedded paleosols within the dune system. Paleosols are a known repository for Sahara Dust, which has a significant impact on the geochemical makeup of sediments. This study used X-Ray fluorescence (XRF) and grain size analysis to detect the presence of Sahara Dust, grain size, and geochemistry within the study area. The grain size analysis showed a possible paleosol in Location 2 but no statistically significant results in Location 1. The geochemistry of the first location showed no real significance either. Geochemical analysis on four samples from Location 2 showed three distinct sediments. In the second location findings indicate the presence of elements found in Sahara dust.

TABLE OF CONTENTS

LIST OF FIGURES

LIST OF SYMBOLS AND ABBREVIATIONS

STSS- South Texas Sand Sheet

XRF- X-ray Fluoresce

Mg-milligram

Tg- Teragram

wt. – Weight

µm– micrometers

PCA- Principal Component Analysis

CHAPTER I

INTRODUCTION

Sahara dust movement

Eolian events create and transport Sahara dust. Local winds determine the amount of Sahara dust that enters the atmosphere (Harrison et al., 2001). Sahara dust enters the atmosphere as saltation load after sandblasting of bedrock surfaces occurs. Saltation drives the creation of dust when finer feldspar and clay grains abrade the surface of sand grains. As the dust particles saltate, they gain height. Eventually, a large dust plume gathers and strong winds blow dust even higher into the air (Harrison et al., 2001). The dust finally reaches the Sahara Air Layer, a strong Atlantic trade wind which transports it to the U.S.A. (Harrison et al., 2001).

There is evidence of Sahara dust distribution occurring for thousands of years, which can be seen in stratigraphic layers (Harrison et al., 2001). Often, dust events decrease visibility and affect air quality (Sakhamuri and Cummings, 2019), but they also alter ecosystems as they augment soils with foreign nutrients. Sahara dust has been confirmed in Amazonian soils in South America (Muhs et al., 2013). In the USA, Sahara dust is present in soils as far west as Utah in the Great Basin (Hahnenberger and Nicoll, 2014) and as far north as Delaware (Fischer and Sarnthein, 1988). Sahara dust has been found in soils but not in sand dunes. This is mentioned in Muhs et al., 2007, because dunes are affected by aeolian processes that would move these small particles. However, dunes have been known to grow vegetation, and these plants could capture small dust particles. Over time, these plants can be buried and form paleosols below the surface and

therefore, it is in these paleosols that Sahara dust has the highest probability of being found (Muhs et al., 2007).

Significance, Research Question, and Objectives

Sahara dust has been found in soils within the USA (Muhs et al., 2007). However, it has not been researched in paleosols or sand dunes. The presence of Sahara dust is beneficial to the soils by providing them with nutrients but in the air, it can be quite harmful to human health. Sedimentological research in the area of the South Texas Sand Sheet is limited, specifically to the potential presence of Sahara dust. Motivated by the limited number of studies in the area, the main research question can be formulated as the following:

Can combined grain size and XRF analysis support in the identification of Sahara dust in paleosols?

To evaluate the research question, the following specific objectives were formulated.

Specific objectives.

- To determine the presence of paleosols via grain size.
- To determine if XRF can show geochemical changes related to paleosols.
- To determine if samples in paleosols contain Sahara dust.
- To determine if XRF can show specific elements in Sahara dust.

CHAPTER II

BACKGROUND

Sand dunes

According to Huggett (2018), a dune is a hill of sand created by wind currents. There are five distinct classes of dune: barchan, transverse, longitudinal, star, and parabolic. Dune morphology is affected by several factors, but the main ones are variance in grain size and shape, the vegetation present within the dune system, and the strength and pattern of winds. Parabolic dunes are formed when there is a regular supply of sand and vegetation, and the wind is neither strong nor mild (Huggett, 2018). Crescent and transverse dunes are created with high to medium sand supply, low vegetation, and mild to medium strength winds (Huggett, 2018). Longitudinal dunes are created with low sand supply, high wind strength, and any amount of vegetation (Huggett, 2018).

Grain Variance

A critical factor in dune morphology is grain size distribution and shape. Wind action is the driving force behind the variance in grain size and shape (Langford, 2015, Bourke et al., 2009). This variance is evident, even within the stoss and lee sides of a dune, with smaller grains residing closer to the dune's crest and larger grains found on the stoss of the dune (Langford, 2015).

Influence of vegetation on dune morphology

The presence of vegetation has a stabilizing effect on sand dunes (Pilkey et al., 2011). The clustering of grasses on dunes affects the shape by dictating the areas of overwash and stabilization (Pilkey et al., 2011). After grasses stabilize dunes, a variety of

plant life can begin to grow and the diversity of plant life indicates how long the dune system has been stabilized (Pilkey et al., 2011).

Influence of wind on dune shape

Wind velocity and frequency directly affect the development of dune shape. Wind causes stress to the surface of a sand dune, and the greater the stress, the greater the change (Huang et al., 2014). The greater the velocity of the wind, the larger the particle size that can be moved (Gao et al., 2015).

Paleosols

Paleosols, or fossil soils, lay below more modern sediments (Kraus,1999). Sand dunes bury vegetation as they migrate, and the buried vegetation becomes soil through pedogenesis (Tabor et al., 2017). The process of pedogenesis turns unmodified sedimentary substrate into paleosol-rich soil, usually during a time of system stability (Tabor et al., 2017). This happens as the weathering and development of soils and sediments change the morphology over time. Subsequent burial and diagenesis cause paleosol creation over time (Tabor et al., 2017). Buried soil horizons become paleosols as diagenesis alters their physical and chemical characteristics. Paleosols are usually classified using the Mack classification system, which looks at organic matter, thickness, number of horizons, redox indicators, in situ mineral alteration, soluble materials, and illuviated insoluble materials (Tabor et al., 2017).

Playas

Playas are dry lake beds primarily found in desert regions. Playas were once active lakes; over time, the lakes dried up to become dry beds (Bowen and Johnson, 2012). These depressions are found in the lowest point of desert basins (Goudie and

Wells, 1995). Evaporation is a contributing factor to playa development. Wind deflation can also help produce playas and, in conjunction, downwind dunes (Bowen and Johnson, 2012). Aeolian processes also transport clastic sediments into the playas. With both clastic and non-clastic deposits, alternating sequences create an impermeable surface (USGS, 2004).

Many playas were lakes and marshes active during the last glacial period. These lake beds dried up around 8000 years ago and often only fill during periods of high floodwater runoff (USGS, 2004).

Large playas often contain dry sediment-dominated sections and damp salt-dominated sections (USGS, 2004). Playas are semi-permanent depositional landforms created by aeolian processes and sediment deposition which can be used to interpret stratigraphy and geomorphic changes (Cooke et al., 1993).

Sahara Dust

Sahara dust deposition depends on wind direction, velocity, and storm event length (Perdikatsis,2010). Sahara dust travels in large plumes, transported by the Saharan Air Layer one mile above the Earth's surface. Plumes of Sahara dust typically arrive in the continental USA during the spring and fall.

Prevailing wind currents commonly move Sahara dust in a westward path across the Atlantic Ocean. Evidence of Sahara dust exists in the Americas, the Caribbean, and Northern Europe (Muhs et al.,2013).

Sahara dust plumes can vary from 100 to 1500 miles in length and travel as far as 5000 miles in a week. In June of 2020, the most extensive plume of Sahara dust over the

Atlantic Ocean was over four times the length of the largest previously observed plume (Colarco,2020).

Sahara dust rapidly falls out of suspension as it reaches the Intertropical Convergence Zone (ITCZ) (Colarco, 2020). The ITCZ is an area of low pressure generated by the convergence of northern and southern trade wind belts (Rodriguez-Navarro, 2018). The ITCZ affects rainfall, droughts, and climate as it migrates north and south of the equator seasonally (Rodriguez-Navarro, 2018).

Sahara dust tends to have a particle range between 40-50µm (Williams et al., 2016), which can cause respiratory issues. In addition, the process of being transported, Sahara dust absorbs and refracts solar and longwave radiation (Harrison et al., 2001).

Often, dust events also decrease visibility and air quality. Sakhamuri and Cummings, 2019, showed that 180 tons of Sahara dust reach the Sahara Air Layer each year. The dust events in 1996-2001 averaged between 15-90 dust events a year globally (Laurent et al., 2008) and the dust ranged from 240Tg to 524Tg (Laurent et al., 2008). There has been a 25% increase in dust events since 2002.

Sahara dust levels have steadily increased within the last 26,000 years (Williams et al., 2016). Williams et al. (2016) concluded that sea temperatures affect the amount of dust transported, and the lower the sea temperature, the less the dust is transported (Williams et al.,2016). Dust ranges were 40-50% lower in the past than that in 2016 (Williams et al.,2016).

Sahara dust is an essential source of nutrients for many environments like the Brazilian Rainforest and the Bahamas (Westrich et al., 2016). According to Prospero and Mayol-Bracero (2013), arid regions in North Africa are estimated to emit ~ 800 Tg yr^{-1} of

soil dust. Sahara dust is rich in iron, aluminum, silica, and phosphorous and contributes to vegetation on land. It can also provide micronutrients to the oceans, generating new growth (Muhs et al., 2013). Unfortunately, this also causes toxic algal blooms to develop and grow, and some of the bacteria transported on the dust can kill corals (Westrich et al., 2016).

Dust could promote a richer habitat for new plant growth in arid environments due to organic nutrients entering the soil (Westrich et al., 2016). Sahara dust is a byproduct of desertification and results in biogeochemical cycling that promotes new growth in other ecological settings and regions.

Sahara Dust Creation

There is evidence of Sahara dust redistribution occurring for thousands of years in the recent past (Prospero et al., 2002). The reason for Sahara dust production and transportation is the Sahel climate and, more recently, climate change. According to Koohafkan, 1996, the Sahel is an area of semi-arid grasslands which divide the Sahara Desert and Sudanian savanna. The Sahel is a hot, dry, and windy area. It has a very low precipitation level, with annual precipitation ranging between 100mm to 200mm (Koohafkan, 1996). Dust storms occur for an average of 100 days a year, and a single storm may travel over 4000 km. Due to accelerated desertification of the region and resulting higher soil erosion rates, dust storm frequency has been increasing as well.

Michaelades, 2019, found that desertification of the Sahara Desert is caused by human activities and climate change, as it is found in areas experiencing significantly less rainfall than before. Areas affected by desertification often lose vital nutrients such as phosphorous and nitrogen. According to Michaelades, 2019, the IPCC

(Intergovernmental Panel on Climate Change) report indicates that the warmer conditions of the Earth have increased the desertification and lowered nutrient levels.

According to Stringer, 2019, the IPCC also reports, that exploitation of natural resources has also increased desertification. In the last hundred years, dust events have increased by 25% due to climate change and changes in land use. According to Stringer, 2019, increased dust in the atmosphere has caused the temperature in the upper atmosphere to rise and, in turn, it is increasing the temperature of the Earth and contributing to climate change.

Sahara Dust in the Atmosphere

Laurent et al., 2008, showed the directionality of Sahara dust using AERONET and NOAA-20 satellites to track the movement and amount of Sahara dust in the atmosphere. From 1996 to 2001, the dust ranged from 585 to 759 Tg. The trajectory was in three different directions, westward, eastward, and northward from the Sahara Desert. Using weather models, it was established that the Sahara dust travels in the Sahara Air Layer to different areas throughout the year. Travel westward occurs mainly in the summer, with the most extensive output happening in May through July and fluctuates between 130 and 1600 Tg (Laurent et al., 2008). Travel northward happens mainly from November through March, whereas travel eastward is in the spring.

Geochemistry of Saharan Dust

According to Perdikatsis, 2010, Sahara dust in Greece contains quartz, illite, albite, kaolinite, palygorskite, dolomite, calcite, and occasionally, smectite and gypsum. Quartz averaged 22 wt. %, the illite 30 wt.%, albite 10 wt.%, kaolite 7 wt.%, palygorskite 4 wt.%, dolomite 4 wt.%, and chlorite, smectite, gypsum around 5 wt.%. Meola,

Lazzaro, and Zeyer, 2015, reported that Sahara dust from the north and west contains a higher percentage of illite in contrast to dust from the south, which contains a higher percentage of kaolinite. In the study of Muhs et al., 2007, paleosols in the Bahamas and Florida contain kaolinite, chlorite, quartz, and gypsum as indicators of Sahara dust, but found that microcline and plagioclase were also present. The amount of African dust found in the sample areas in the Bahamas was between 20µm to 40µm, and between 30-120 ppm based on the month of the year (Muhs et al., 2007).

Geological History of the South Texas Sand Sheet

During the Mesozoic Era (252-66 Mya), the Ouachita Mountains separated from the North American plate due to uplift; this developed the coastal plains of Texas (Baker, 1995). The Gulfian tectonic cycle is a cycle of several periods of continental extension or rifting and compression (Baker, 1995). Extension and compression created an oceanic basin as the plates separated during the Triassic (252-201 Mya) (Baker, 1995). Marine salts covered the rift basins in the Gulf coast basins. These were then covered by igneous rocks that formed the Gulf coast basin (Baker, 1995). Deposits of carbonate shelf and delta sandstones and shales deposited in the basin, creating the Gulf coast. Salt domes formed during the Jurassic Period (201-145 Mya) and created oil and gas traps (Fulbright et al., 1990). During the Cretaceous (145-66 Mya), seas covered much of Texas.

At the beginning of the Cenozoic (66 Mya to present), uplift during the Laramide orogeny drained the seas from much of Texas (Fulbright et al., 1990). The deltas prograded the Gulf coast, and sediment deposits increased considerably in these areas, creating more salt domes (Fulbright et al., 1990). The uplift continued to rise in central

Texas and caused subsidence in the Gulf coast. Coastal subsidence led to the creation of the Balcones fault zone (Saribudak, 2015).

During the Tertiary, erosion of sedimentary rock and uplift of central Texas allowed for the exposure of the Pilot Knob volcano (Saribudak,2015). After this, in the late Cenozoic (34mya), large amounts of sand and gravel accumulated in the Texas panhandle (Baker, 1995). Alluvial deposits created a sheet to the east as river drainage from the west occurred. The ice cap expansion advanced and retreated, causing a change in sea level in the Gulf of Mexico (Saribudak, 2015). These transgressions and regressions were a result of warming and cooling periods (Saribudak, 2015).

During the Quaternary, dunes dominated North America (Forman et al.,2009). There were multiple dune deposit events that reworked the sediments during the Holocene (11650ya-0ya) (Forman et al.,2009). Dune reactivation is currently ongoing in the semi-arid grassland area of South Texas. South Texas includes the inner belt (Blackland Prairies), the lowland plain (interior plains), and the upper Cretaceous coastal plains regions (Figure 1) (Baker, 1995). The high southern plains have been reactivated several times in the last 4000 years, with the last dune activation being around 600 years ago (Muhs and Holliday, 1995).

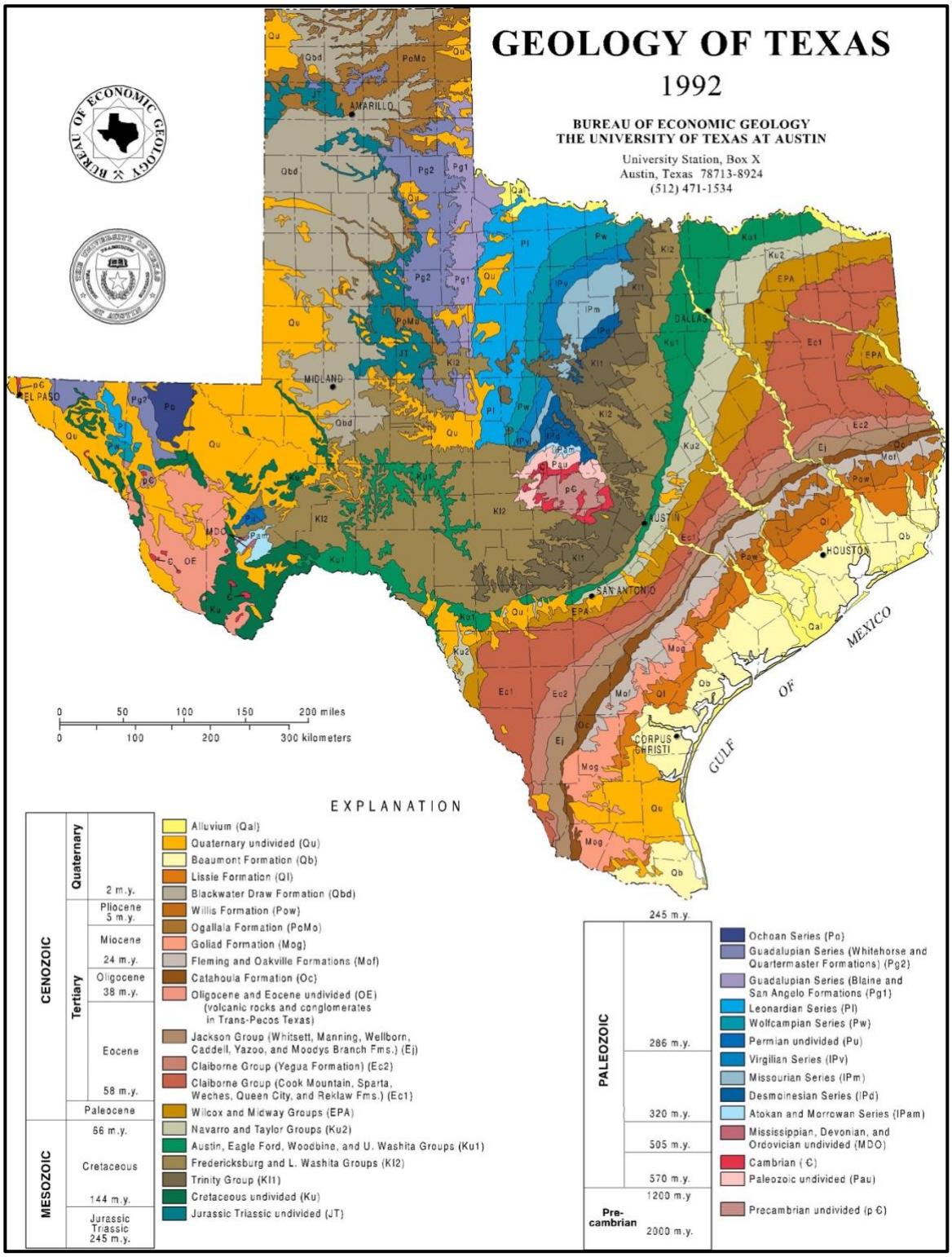

Figure 1. The stratigraphy of Texas (Bureau of Economic Geology, 1992).

CHAPTER III

STUDY AREA

Texas Playas

Playas account for 2 percent of the Texas plains (TPWD, 2021). There are close to 20,000 playas throughout the Texas plains. Playas are often large in Texas, ranging from 15 acres to 800 acres (TPWD, 2021). Most playas are found on farmlands leading to decreased water levels and higher levels of sedimentation due to the poor recharge occurring at these playas (TPWD, 2021). Alternatively, buffers of grasslands around playas have been increased to lower incoming sedimentation and to increase recharge, preserving the water within active playas in the Texas plains (TPWD, 2021).

The prairies of coastal Texas disappeared during the Holocene as the climate changed from humid to arid. Reactivation events buried vegetation located on dunes during periods of stability (Baker, 1995). Therefore, it is highly probable that paleosols exist beneath dune surfaces.

Local Studies at the Kenedy Ranch Sand Dunes

The South Texas Sand Sheet on the Kenedy Ranch located in Kenedy County is over 120 acres covered with remnants of sand dunes (Figure 2). Climatic drying periods during the Holocene created the STSS of quartz-rich sands. There have been several drought periods during the past 1,000 years.

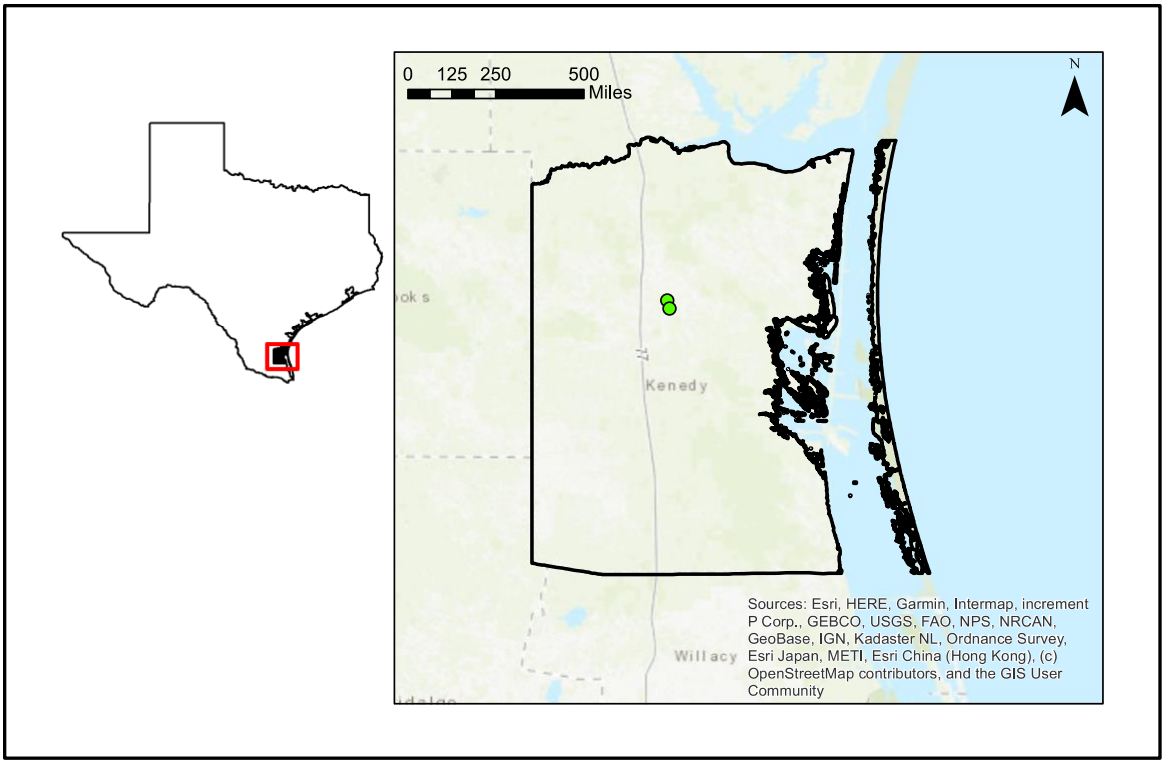

Figure 2. Location of the Kenedy Ranch Sand Dunes in Texas and within Kenedy County.

The prevailing wind comes from a southeast direction which would support the possibility of Sahara dust being present (Forman et al.,2009). In the spring, summer, and fall, the wind comes from the southeast with an average of 9m/s, 6m/s, and 6m/s, respectively (Forman et al., 2009). In winter, the wind comes from the south and north with an average of 9m/s (Forman et al., 2009).

The Kenedy Ranch dunes are parabolic in nature and bidirectional in the southeast and northwest (Forman et al., 2009). Studies by Forman et al. (2009) date the sheet as 3000 years old. However, newer studies date the sand sheet at close to 6500 years (Barreau et al., 2017).

Forman et al. (2009) studied two locations; Site one (27° 7′ 55.3″ N; 97° 28′ 30.1″ W) and Site two (27° 8′ 36.01″ N; 97° 42′ 19.58″ W). These locations were on the King Ranch just outside Sarita, Texas. The King and Kenedy Ranch are neighboring ranches that are both in Kenedy County. Forman et al., 2009, dated the sand at these locations to be Holocene in age and found paleosols at each of the sites. Forman et al. (2009) generated a stratigraphic column for the study area by carbon dating samples and found paleosols dated at 200 years old. The pedogenesis contact begins below the sand dunes that were dated at 10-95 years old (Forman et al., 2009).

Specific Sample Site Locations

The locations from Forman et al., 2009 were not available to this study due to the division of the land on the ranch. Therefore, the two locations (Figure 3) used for this study were located nearby the locations from Forman et al. (2009) due to their spatial proximity and being part of the South Texas Sand Sheet.

Figure 3. Sample collection in playa, referred to as Location 1 (27.0273, -97.7478), and in dune, referred to as Location 2 (27.0148, -97.7435). Both samples were collected at the Kenedy Ranch in Kenedy County, Texas.

The set of samples was collected at the edge of a playa, referred to as Location 1. The coordinates in decimal degrees are 27.0273, -97.7478 with elevation of approximately 6m above mean sea level. The stratigraphy is Quaternary in age. Four separate trenches were dug onto the side of the playa due to the slopped edge of the

surface, and samples were divided into four different groups (Figure 4). The trenched areas were named 1A (top), 1B, 1C, and 1D (bottom).

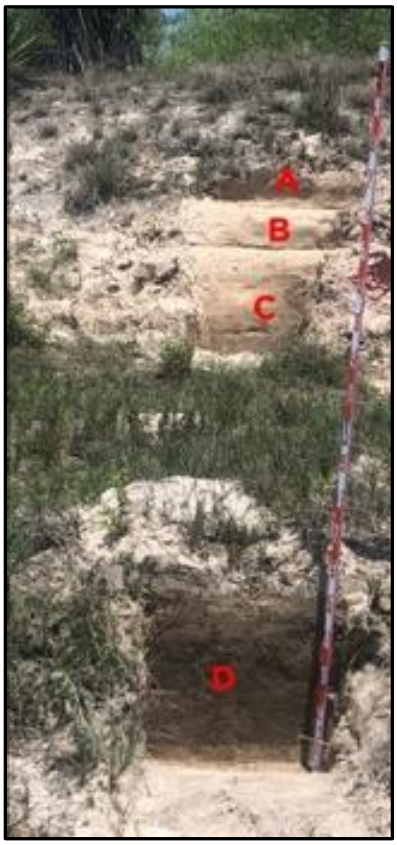

Figure 4. Location 1 trenches 1A, 1B, 1C, and 1D dug at the playa.

The second set of samples was collected in an arm of a parabolic dune situated on the ranch, referred to as Location 2. It is located on the West Gulf Coastal Plain stratigraphy. This site has coordinates in decimal degrees of 27.0148, -97.7435 and elevation of approximately 10m above mean sea level. The sand is Quaternary in age and appears to be sand sheet deposits. The location seems to show a gleied area at the bottom of the dune which appears to be a paleosol, followed by crossbedding, and lastly, an

eolian sand dune at the top. The samples were collected 5cm from the bottom, up to the top 190cm in height, which was the surface (Figure 5).

Figure 5. Collection of samples in dune using trench measured from 5-195cm and referred to as Location 2. Located at the side of a parabolic dune on the Kenedy Ranch, Kenedy County, Texas.

CHAPTER IV

METHODS

Field Data Collection

Samples at the study area were collected, utilizing small excavation trenches dug by hand to expose the stratigraphy of the playa and dune. Collection of samples from exposed stratigraphy was performed at 5 cm intervals to identify distinct stratigraphic units (SU) and erosional boundaries. Samples were collected and stored for transportation in individual Ziploc® bags and labeled with depth below the surface and corresponding geographic coordinates.

Grain-size Analysis

Mastersizer 3000E

Grain size varies between the stoss and crest of a dune and vertically through a dune. A Malvern Panalytical Mastersizer 3000E (Figure 6), equipped with a Hydro EV dispersion unit, analyzed grain size distribution in samples collected from the study area.

Figure 6. The Malvern Mastersizer equipment used.

The Mastersizer 3000E can detect 100 user-adjustable size classes ranging from 0.1 – 1000 microns, with an accuracy better than 0.6%, precision and repeatability better than 0.5% variation, and reproducibility better than 1% variation, all of which is dependent on the recovery of the mean size of a narrow log-normal distribution and sample preparation (Collins et al., 2018). The mastersizer uses laser diffraction to scatter light through the sample. This is analyzed to calculate the size of the particles creating the scattering. Sediment samples were prepped for analysis on the Malvern following Collins et al. (2018). Preparation includes sieving, mixing the sediments with distilled water, and deflocculation if the sediment contains clays.

Preparation and methodology

The samples from the playa at Location 1 contained carbonates. In the time it took for the samples to be analyzed, they had hardened and therefore could not be separated, so they had to be treated with 25% HCL before deflocculation. All samples were treated with deflocculation solution to break down the clays within the sample to be analyzed. The beaker was filled with 400ml distilled water. The mastersizer was set to analyze quartz spherical crystals and measured in µm. Due to the size of the samples being below 5mg, the obscuration level was dropped to between 10-20%. The samples were run three times to get an average. The mastersizer was cleaned between samples to stop contamination. The samples from 190cm to 45cm found in location 2 did not have to be treated with deflocculation solution since the samples were visibly high in sand content. The samples found below 45cm were treated with deflocculation solution because of the gleied nature of the bottom section of the sand dune.

Geochemical Analysis using the XRF Spectrometer

Handheld XRF

The use of X-ray fluorescence provides the means to determine geochemical properties of samples. X-ray fluorescence (XRF) (Figure 7) looks at the protons of elements within a sample to determine its geochemical properties. According to Spectro, 2021, XRF uses an intense x-ray beam, usually from an Rh target; it excites the sample, ionizing and exciting its electrons. As ionization occurs, atoms within the sample release unique emissions. The scintillation detector sees short-wavelength emissions, while the flow counter sees long-wavelength emissions (Spectro,2021).

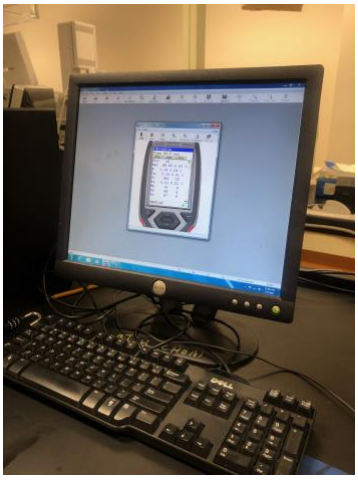

Figure 7. Handheld XRF device.

Sediments were sieved using nested sieves, ranging between no.18-400 until the samples were below 40µm based on previous studies (Muhs, 2013). Dry sieving of samples was the least destructive sample preparation method. The XRF sample must be

within 100-500mg for accurate analysis, and samples from 0.1g to 3.0g are needed to fill the sample holder. Samples are ground into a fine powder with a mortar and pestle in preparation for analysis. The operator places powdered samples on microscope slides in random orientation. The operator places the ground sample into the holder, then places the XRF film on top and seals it using the cap and collar. Next, the operator selects soil mode on the XRF machine and enters metadata for the sample. It is essential to align the sample and screen of the XRF machine and set the internal timer (Spectro, 2021). After analyzing the sample, the user interface on the XRF machine will display the elements, concentration, and error of measurement.

Preparation and Methodology

The samples were weighed out to 2g each. They were then put in the plastic sample holders and covered with a film used for XRF. The XRF was housed in a protective box to stop the radioactivity from escaping. The sample was tested for 240 seconds, and all geochemistry elements were tested. Location 1 and 2 were tested primarily for the geochemical makeup of the playa and sand dune, respectively. The samples from location 2, which contained clay-sized grains, were sieved to be analyzed for Sahara dust. The samples were between 0.1g to 1.0g of dust material. The sample had been previously sieved through a 40µm sieve. Four samples at 15cm, 20cm, 25cm, and 30cm from location 2 contained enough dust to be tested. The standard reference minerals indicating the presence of Sahara dust are quartz, illite, albite, kaolinite, palygorskite, dolomite, calcite, and occasionally traces of smectite and gypsum (Perdikatsis, 2010 and Muhs et al., 2007).

CHAPTER V
RESULTS AND FINDINGS

Grain-size Analysis

Location 1 - Playa

Results from the mastersizer analysis were presented based on particle sizes of clay, silt, and sand (Figure 8). This was accomplished by using the thresholds of 0.1µm, 0.1µm to 60µm, and 60µm to 2000µm, for clay, silt, and sand, respectively. The results were then divided into percentages and graphed. It can be seen from the results that the grain sizes seem to be very similar throughout the profile depth. The average for all depths appears to be close to 25% clay, 50% silt, and 25% sand. The results do not appear to show any significant trends or any sign of a paleosol in this location. There does seem to be an anomaly at 1C 55cm. Even though grain sizes do not show significant changes in grain size with depth, the XRF geochemical analysis at the playa may differ.

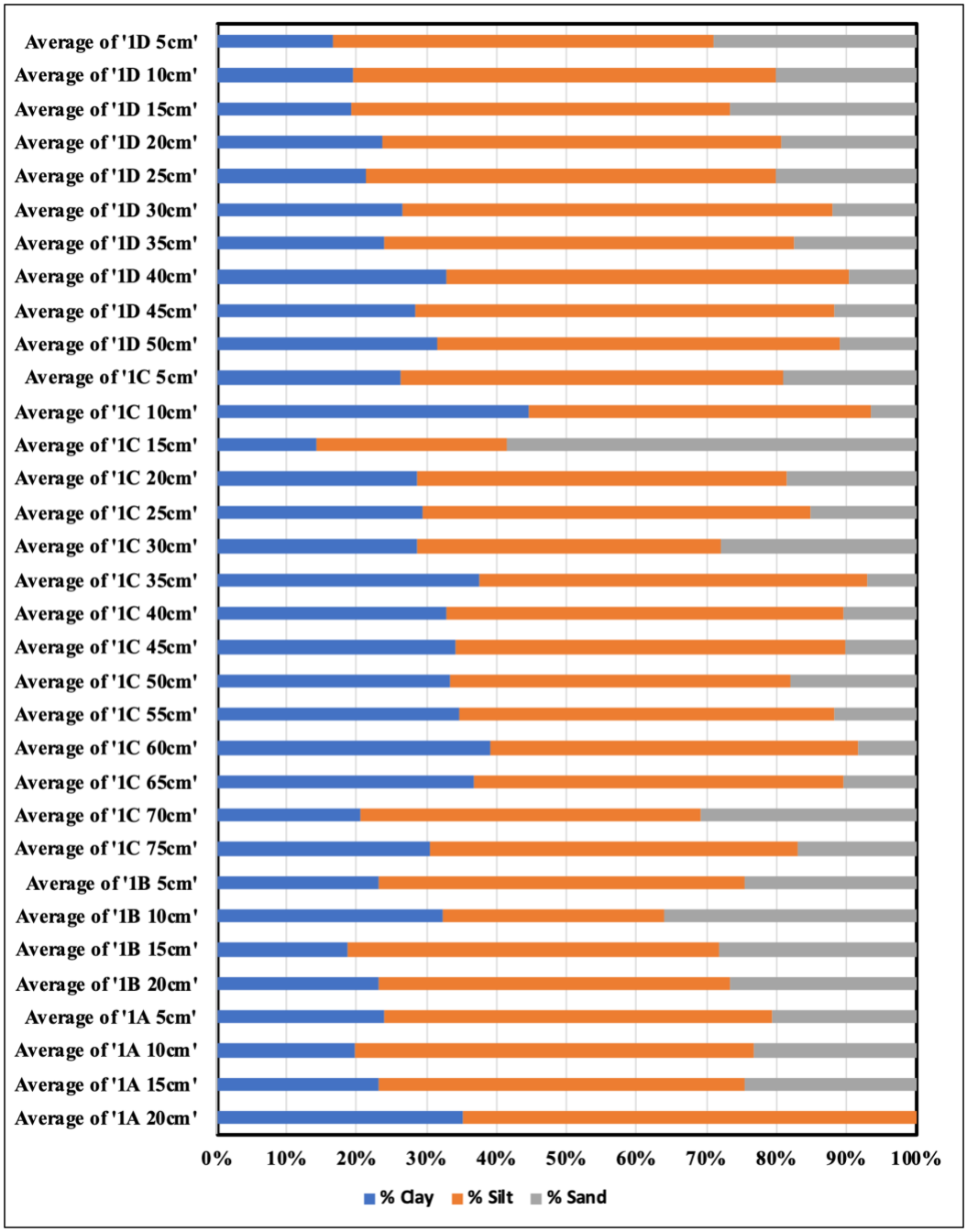

Figure 8. Grain size results in percentages of sand, silt, and clay at all depths. These are from trenches 1A, 1B,1C, and 1D at the playa Location 1, on the Kenedy Ranch.

Location 2 - Dune

Location 2 was analyzed from the base at 5cm to the surface at 195cm (Figure 9). The analysis below 5cm could not be performed due to rising water filling the trench. The surface to 40cm shows mostly sand with only about 1-2% silt and no clay. At approximately 40cm there is a significant change in grain size and type of particles. There is 40% clay, 50% silt, and 10% or less sand. This suggests that this area could have different geochemistry than the rest of the sand dune. This appears to be significant as we can see a trend of fining downward in the dune from the surface down to 35cm. There is also a change in particle distribution as we descend downwards through the dune, especially below 35cm.

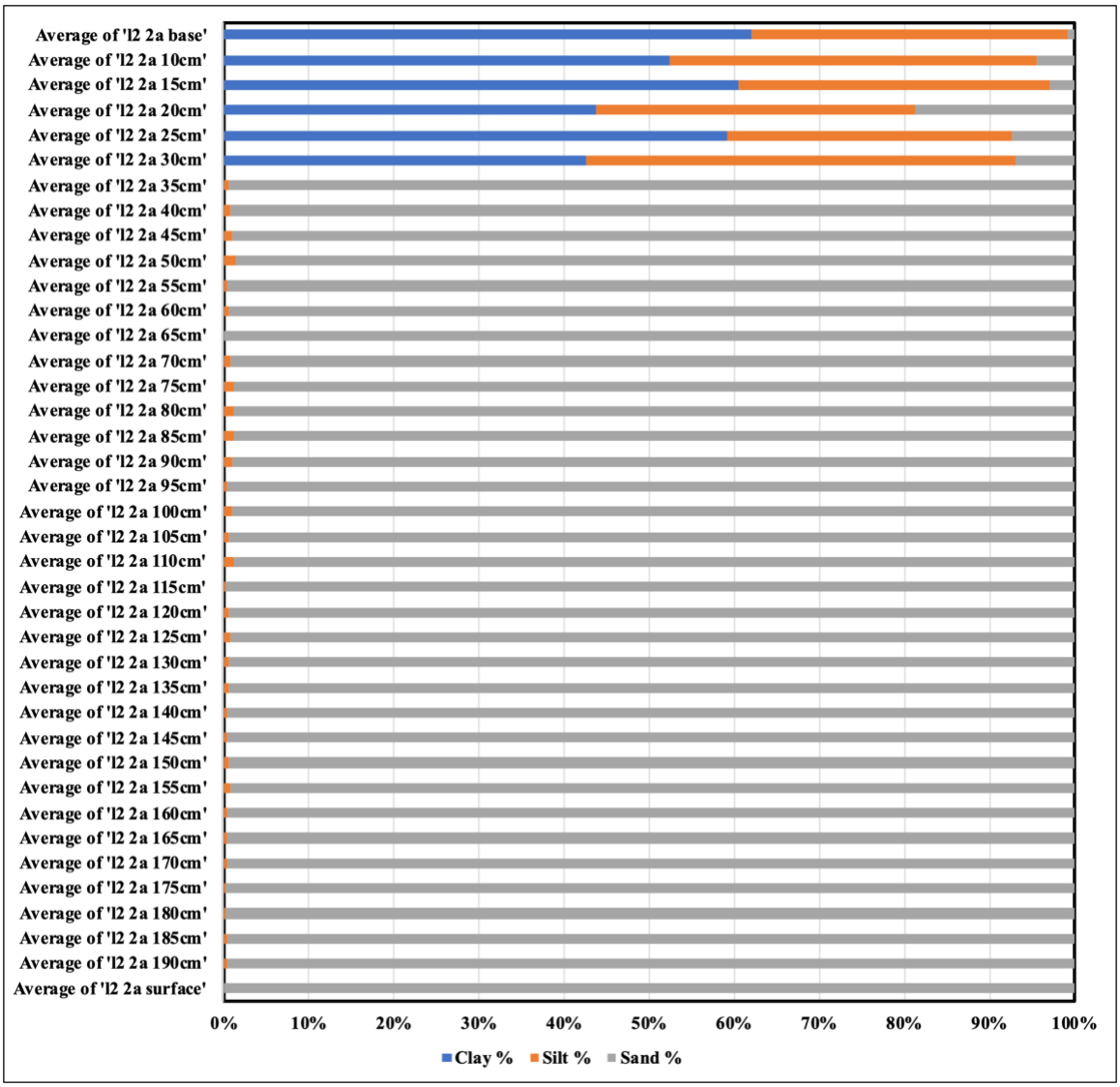

Figure 9. Grain size results at the parabolic dune, Location 2, from 5cm to surface, showing the percentages of sand, silt, and clay.

Geochemical Analysis using the XRF Spectrometer

Location 1 - Playa

The XRF analysis was performed on all samples at all depths from location 1. The results outside the standard error and above the limit of detection (LOD) were plotted (Figure 10). These elements were molybdenum, zirconium, strontium, rubidium, arsenic, zinc, iron, chromium, titanium, calcium, potassium, and niobium. The XRF data points were plotted in terms of the location and concentration of the element. This location showed two changes, at around 1D 50cm and 1A 20cm. Peaks can be observed at both points on multiple element graphs. According to the geochemical results, the samples at this location are mostly comprised of calcium, potassium, and iron.

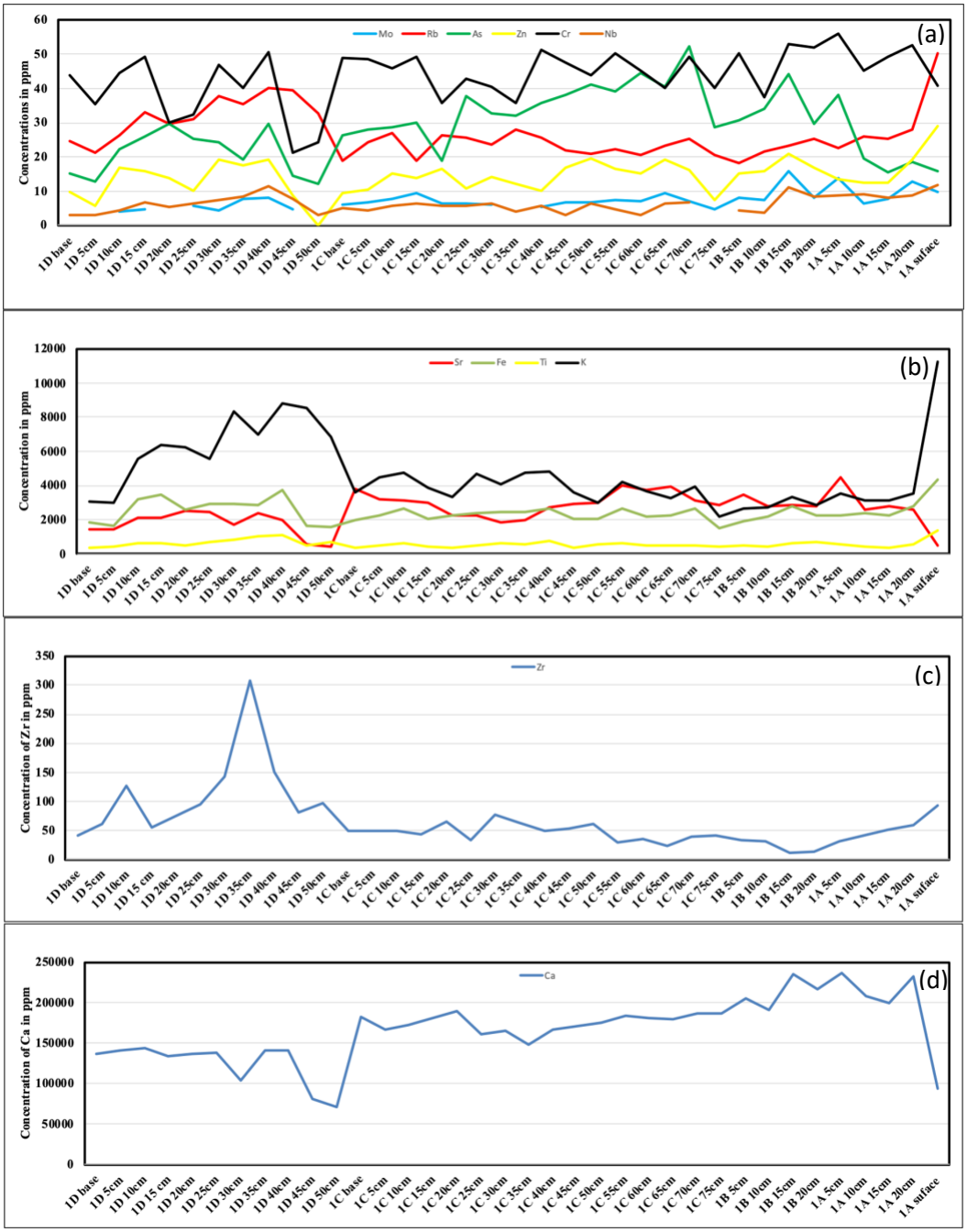

Figure 10. Measured concentration of key elements from XRF analysis for Location 1 (playa). Due to the different scales, these results were organized in different graphs. Elements of molybdenum, rubidium, arsenic, zinc, chromium, and niobium (a), strontium, iron, titanium, and potassium (b), zirconium (c), calcium (d).

Location 2 - Dunes

Similar to location 1, XRF analysis was performed on all samples from location 2 (Figure 11). The elements graphed included zirconium, strontium, chromium, rubidium, iron, titanium, scandium, calcium, potassium, sulfur, and niobium. The geochemistry seems to indicate that there are three separate sections. The first section seems to be from samples in depths from 10cm to 40cm, the second section from 45cm to 120cm, and the final section was from 125cm to the surface (195cm). This is evident in the graph of strontium (Figure 11d). The XRF element concentration graphs show a higher element concentration from 10cm to 40cm. The concentration drops in the center before rising again in the final section of 125cm and above. The highest concentrations were calcium, scandium, and potassium. The bottom section also had a high amount of iron and sulfur compared with the rest of the dune.

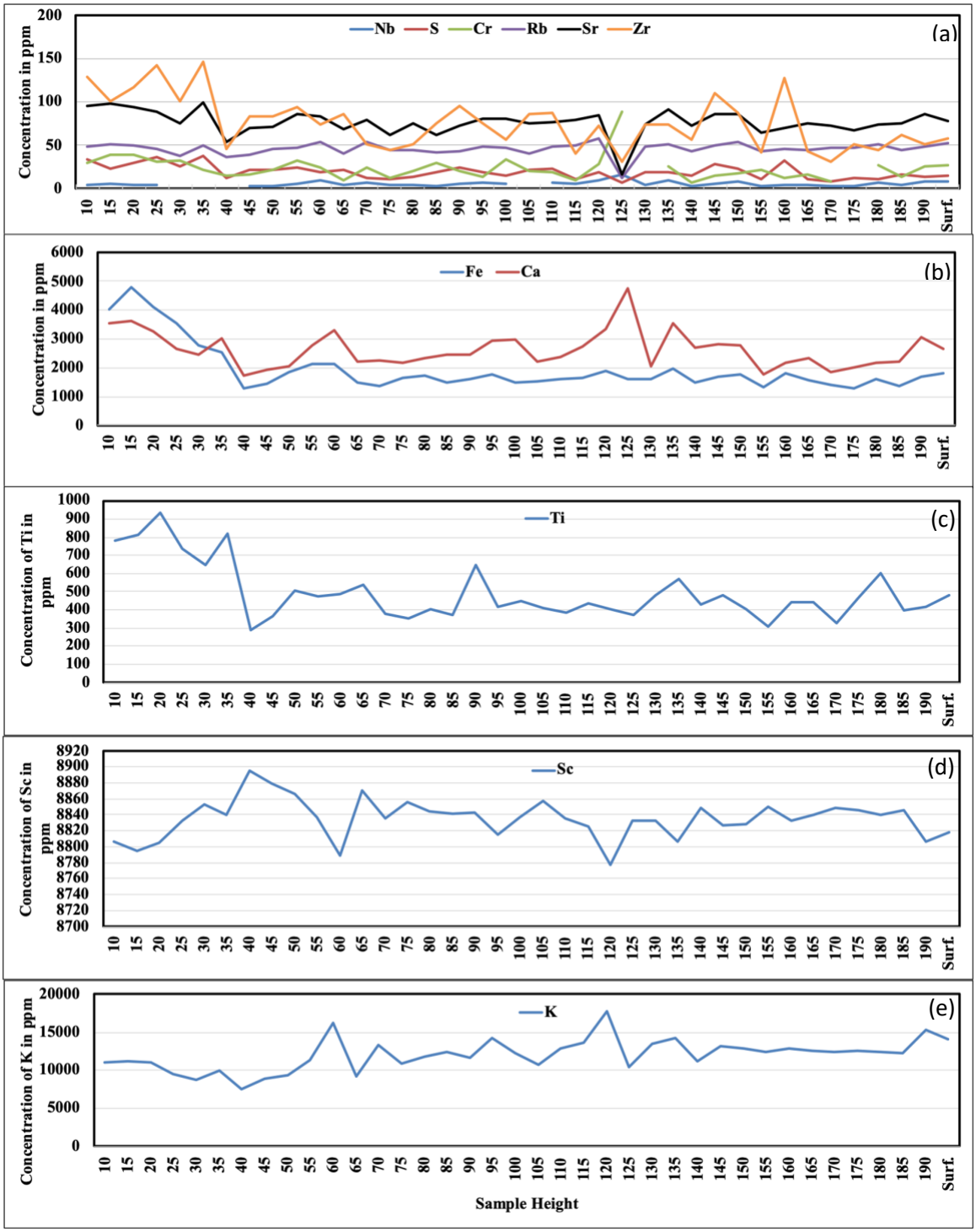
(a)
Nb
S
Cr
Rb
Sr
Zr
Concentration in ppm
(b)
Fe
Ca
Concentration in ppm
(c)
Ti
Concentration of Ti in ppm
(d)
Sc
Concentration of Sc in ppm
(e)
K
Concentration of K in ppm
Sample Height
Surf.

Figure 11. Measured concentration of key elements from XRF analysis for Location 2 (parabolic dune). Elements of niobium, sulfur, chromium, rubidium, strontium, and zirconium (a), iron, and calcium (b), titanium (c), scandium (d), potassium (e).

Geochemical Analysis of Dust

According to Muhs et al., 2009, dust particles are below 40 micrometers in size. The samples at Location 2 were sieved through a 40µm sieve. The dust was found at multiple depths, but only concentrations found at 15cm, 20cm, 25cm, and 30cm the XRF could be used in the XRF analysis (Figure 12). The elements measured by the XRF machine at traceable amounts were molybdenum, zirconium, strontium, rubidium, arsenic, zinc, copper, iron, manganese, chromium, vanadium, titanium, scandium, calcium, potassium, sulfur, and niobium. Element concentrations start low at the lowest depth, then rise and level off around 25cm, before finally falling until it reaches the 30cm depth.

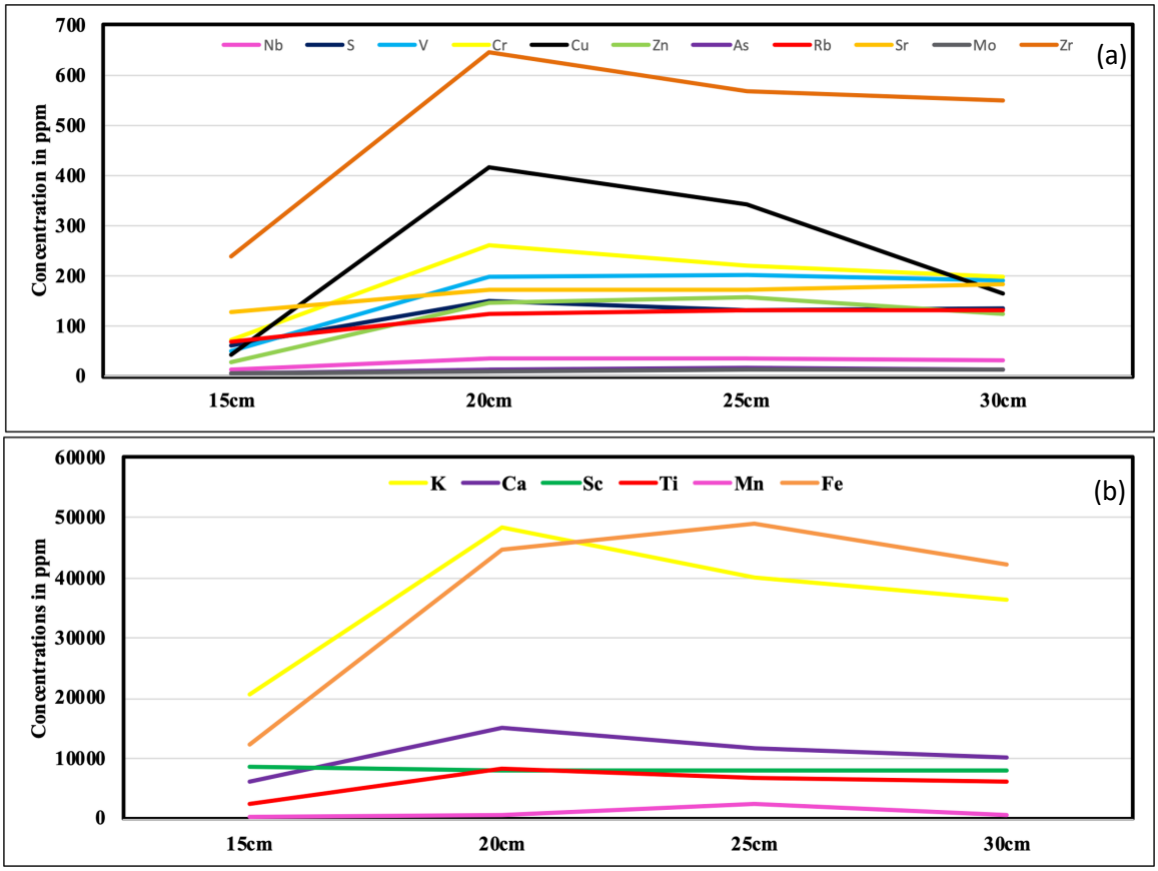

Figure 12. Measured concentration of key elements from XRF analysis of dust at Location 2 (parabolic dune). Due to the different scales, these results were organized in different graphs. Elements of niobium, sulfur, vanadium, chromium, copper, zinc, arsenic, rubidium, strontium, molybdenum, and zirconium (a), potassium, calcium, scandium, titanium, manganese, and iron (b).

CHAPTER XI

DISCUSSIONS, CONCLUSIONS, AND RECOMMENDATIONS

Discussion

The original purpose of this study was to investigate if Sahara dust could be found in paleosols at the South Texas Sand Sheet. The objective was to use the grain size analysis to identify the location of the smallest grains in the vertical profile and the geochemistry analysis was utilized to discover where, in the vertical profile, a paleosol was to be tested for Sahara dust.

The grain size analysis from location 1 was insignificant. The playa had almost an even distribution of clay, silt, and sand. Even though the particles were the correct size for discovering Sahara dust, there were no changes in particles from top to bottom in the stratigraphy. There was only one anomaly at 1C 55cm, which could potentially be attributed to data collection/preparation error, such as potential insufficient utilization of deflocculated solution mixed with the water. This, in turn, lowered the levels detected by the mastersizer. As there was no change in particle distribution throughout the vertical column, it can be inferred that there is no paleosol at this location and this could be attributed to the lack of peds at this location (Tabor et al., 2017).

Location 2 did seem to have some significant changes in the particle size distribution in the vertical column. Grain size analysis indicated a reducing grain size downward, with percent of silt size increasing from the surface to the 40cm mark. The particle size completely changes below 40cm, suggesting a change in sediment environment (Bourke et al., 2009). Due to this particle size distribution, it may be possible that these changes indicate a paleosol being present. Previous observations

show these aeolian sands are primarily massive with little internal cross-stratification (Forman et al., 2009). There also seem to be peds at this location (Figure 5).

Results of the grain size analysis between the playa and the dune are vastly different. Findings indicate that the sand dune and playa are not similar in terms of particle size distribution and that the aeolian processes do not create or act in the same way at these locations.

The XRF is a valuable technique for assessing the geochemical properties of sediment samples measured as a depth profile. The machine provides elemental concentrations in ppm. The XRF analysis can generate environmental reconstructions based upon sediment provenance. The XRF handheld machine measured only some elements which significantly impacted the analysis of the data as not all major elements were detected. The machine available to this study had limitations on how the results were presented. Unfortunately, only concentration vs. sample height could be graphed because some samples had results below the detection limit. In addition to some elements having concentrations so high, they did not register on the machine, as was seen with silica.

Location 1 does not seem to have statistically significant XRF geochemistry data. This can be attributed to the complex evolution of playas which makes it hard to interpret their stratigraphy (Cooke et al., 1993). The location does have two unusual peaks at 1D 50cm and 1A 20cm which can be attributed to both being located at the playa's surface. This can be seen in Figure 4, where the terraced area and the sample holes are close to the surface. The high levels of calcium are caused by the calcium carbonate in the shells and limestone of the area, as it was a coastal area that has since regressed. This can be seen

in Figure 1, and it was also mentioned in Hills, 1940. Playas tend to exhibit little horizonation other than strong inverse relationships between Si and Ca, where samples show sudden increases in Ca content associated with smaller grain sizes. This may be influenced by cementation from carbonate muds typical in the study area (Fulbright et al., 1990). The high potassium levels are from the clays, which make up around 25% of the particle distribution (Figure 8). The high levels of iron are harder to explain. The iron is probably from the parent material or some provenance or diagenesis process, which this analysis could not reveal (Kraus,1999). The concentrations of iron may be so high due to its insolubility.

Grain size analysis of location 2 indicated three distinct sections. The site is a recently active dune that revealed enhanced horizonation. This can be seen in the geochemical results and the peaks displayed by elements. Even though silica was not graphed, it is believed that the XRF machine was saturated with the high percentage of silica. The lower section was high in iron and potassium, which is due to the gleied nature of the location and the high clay content. The scandium is probably also a derivative of the clay material. The sulfur may be due to gypsum salts found in the area (Baker, 1995). The middle section shows a drop in the concentration of these elements, probably due to the shift in particle sizes and different geochemistry. The last section shows another increase in potassium and scandium. Again, this increase could be due to the erosion processes in the area, sending gypsum-rich dusts into the air, where they then become part of the makeup of the sand dune (Saribudak, 2015).

Location 1 and 2 are different in their geochemistry but do have elements in common because they both contain clays and silts. Though they contain many of the

same elements, the concentrations are very different. The first location is comprised mainly of calcium, largely due to the carbonate shells found in the sediment. The second location has a somewhat mixed composition. The top is silica based, whereas the bottom is a clay dominant section. The middle suggests a difference in composition, which may be a paleosol as much of the altered physical changes can be seen in Figure 5 (Tabor et al., 2017).

The dust was collected from the bottom section of the sand dune. This was due to no other section containing enough small-sized particles to test. The samples were from 15cm, 20cm, 25cm, and 30cm. Based on studies from Perdikatsis (2010) and Muhs et al., (2007), compounds that would indicate Sahara dust include the following elements: aluminum, silica, calcium, sodium, potassium, magnesium, and iron. The concentration levels are high for the element's calcium, potassium, and iron. Although the presence of these elements does not definitively prove that Sahara dust is present, it provides evidence that the elements that make up the compounds in Sahara dust are present. These findings are significant and can be interpreted as an initial screening to inform whether more complex analysis should be employed to confirm the presence of Sahara dust.

Conclusions

The objectives of this study were to evaluate if Sahara dust can be found in sand dunes at the Kenedy Ranch in Sarita, Texas. Though paleosols can be found in sand dunes, definitive proof of Sahara dust is harder to find. The differences between a playa and a sand dune are significant and show how different aeolian processes affect the composition of the sediment. The first location showed no statical significance when it came to particle size distribution, as the particles were virtually the same throughout the

vertical profile (Figure 8). No real statistical significance was noted in the geochemical analysis using XRF technology, as the peaks were only due to surface results skewing the data.

The second location, however, proved much more significant. Not only did the three changes in geochemistry seem to indicate the presence of a paleosol, but the bottom section also appeared to show that there were enough clay sized particles under 40 micrometers to test for Sahara dust. Though the dust samples indicated the presence of some of the elements which are part of the compounds that make up Sahara dust, it does not conclusively mean it is Sahara dust itself, as these elements make up a great many other compounds. However, the combined grain size and XRF analysis in this study has proven to support investigations designed to quantify the presence of Sahara dust in paleosols. It could be used as the initial step in determining whether more complex geochemical analysis is needed.

Recommendations for future work

When it came to studying Sahara dust, papers could be found on air sampling and Sahara dust, but not on the study of Sahara dust in sand dunes. This may be due to the fact that dust particles move so easily due to aeolian processes. Paleosols, though, are known to trap pedogenic particles, and as they once contained vegetation, it could be true that they could trap smaller particles, such as Sahara dust. This study found the presence of several elements present in Sahara dust. However, the machine's inability to measure all elements that contribute to Sahara dust requires further investigation. Uncertainty was created during the study by the size of the samples and time. With more time, XRD would be able to be performed to show elemental compounds, which could yield more

conclusive results. Both X-ray Diffraction (XRD) and Principal Component Analysis (PCA) could make identifying the compounds remarkably more straightforward. Future research should include larger samples so that better analysis can take place. There is little research on the south Texas sheet and limited research on XRF analysis on playas. Both these subjects could be researched further.

BIBLIOGRAPHY

Baker, E.T. (1995). Stratigraphic nomenclature and geologic sections of the gulf coastal plain of Texas. *US Geological Survey Report* 94-461.

Barrineau, P., Dobreva, I., Bishop, M., Houser, C., and Forman, S. (2019). Deconstructing aeolian landscapes. *Catena*, **174**, 452-468.

Bernal, S., and Bogard, J. (2004). Protocols for Thermoluminescence and Optically Stimulated Luminescence Research at DOSAR, *DOE Report 2004*, 0-45.

Bourke, M.C., Ewing, R.C., Finnegan, D., and McGowan, H.A. (2009). Sand dune movement in the Victoria Valley, Antarctica. *Geomorphology*, **109**, 148-160.

Colarco, P., and Raga, G., 2020, World resources institute air quality. *Tech talks august 6,2020.*

Collins, J.D., Gill, T.E., Langford, R. (2018). Characterizing formation processes of Rimrock Lake, a Late Pleistocene–Holocene playa, Harney Basin, south-eastern Oregon, USA, using an end-member mixing analysis. *Journal of Quaternary Science*, **33**, 721–737.

Cooke, R.U., Goudie, A., and Warren, A. (1993). *Desert geomorphology*, London, UCL Press.

Fischer, A., and Sarnthein, M. (1988). Airborne Silts and Dune-derived Sands in the Permian of the Delaware Basin, *Journal of Sedimentary Research*, **58**(4), 637-643.

Forman, S., Nordt, L., Gomez, J., and Pierson, J. (2009). Late Holocene dune migration on the south Texas sand sheet, *Geomorphology*, **108**, 159-170.

Fulbright, T., Diamond, D., Rappole, J., and Norwine, J. (1990). The Coastal Sand Plain of South Texas, *Rangelands*, **12**(6), 337-340.

Gao, X., Narteau, C., Rozier, O., and Courrech Du Pont, S. (2015). Phase Diagrams of Dune Shape and Orientation Depending on Sand Availability, *Scientific Reports*, **5**, 146-177.

Goudie, A.S., Wells, G.L. (1995). The nature, distribution, and formation of pans in arid zones. *Earth-Science Reviews*, **3**, 1-69.

Harrison, S.P., Kohfeld, K.E., Roelandt, C., and Claquin T. (2001). The role of dust in climate changes today, at the Last Glacial Maximum, and in the future, *Earth Sci. Rev*, **54**, 43–80.

Hahnenberger, M., and Nicoll, K. (2014). Geomorphic and land cover identification of dust sources in the Eastern Great Basin of Utah, USA. *Geomorphology*, **204**, 657-672.

Hills, E.S. (1940). The lunette, a new landform of aeolian origin. *The Australian Geographer*, **3**, 15–21.

Huang, N., Jiang, H., and Zhu, Y. (2014). Analysis of wind-blown sand Movement over transverse dunes, *Scientific Reports*, **2014**, 1-11.

Huggett, R. J. (2018). Sand dunes *in fundamentals of geomorphology, (fourth edition)*, London, U.K. Routledge 372-489.

Koohafkah, A. (1996). Desertification, Drought and their consequences, *SD Dimensions*, 7-11.

Kraus, M. (1999). Paleosols in clastic sedimentary rocks: their geologic applications, *Earth-Science Reviews*, **47**, 41-70.

Langford, R., Gill, T., and Jones, S. (2015). Transport and mixing of eolian sand from local sources resulting in variations in grain size in a gypsum dune field, White Sands, New Mexico, USA. *Sedimentary Geology*, **333**, 184-197.

Laurent, B., Marticorena, B., Bergametti, G., Le'on, J., and Mahowald, N. (2008). Modeling mineral dust emissions from the Sahara Desert using new surface properties and soil database, *Journal of Geophysical Research*, **113**, 1-24.

LeVarge, S. (2005). Applications of Logarithmic and Exponential Functions, *The Biology Project*, Arizona.edu.

Malvern Mastersizer (n.d.). *Malvern Panalytical Mastersizer.* Retrieved December 27, 2021, from www.malvernpanalytical.com

Meola, M., Lazzaro, A., and Zeyer, J. (2015). Bacterial Composition and Survival on Sahara Dust Particles Transported to the European Alps, *Frontiers in Microbiology*, **6**, 1454-1476.

Michaelides, K. (2019). SPMA Contributors to IPCC Special on Climate Change and Land, *IPCC Annex III*, 839-2966.

Moreno, T., Querol, X., Castillo, S., Alastuey, A., Cuevas, E., Hermann, L., Mounkaila, M., Elvira, J., and Gibbons, W. (2006). Geochemical Variations in Aeolian Mineral Particles from the Sahara-Sahel Dust Corridor, *Chemosphere*, **65**, 261-270.

Moskowitz, B., Reynolds, R., Goldstein, H., Berquo, T., Kokaly, R., and Bristow, C. (2016). Iron Oxide Minerals in Dust-Source Sediments from the Bodele Depression, Chad: Implications for Radiative Properties and Fe Bioavailability of Dust Plumes from the Sahara, *Aeolian Research*, **22**, 93-106.

Muhs, D.R. (2013). The geologic records of dust in the Quaternary, *Aeolian Research*, **9**, 3-48.

Muhs, D., Holliday, V. (1995). Evidence of active dune sand on the Great Plains in the19th century from accounts of early explorers. *Quat. Res*, **43**, 198–208.

Muhs, D.R., Budahn, J.R., Prospero, J.M., and Carey, S.N. (2007). Geochemical evidence for African dust inputs to soils of western Atlantic islands: Barbados, the Bahamas, and Florida. *Journal of Geophysical Research: Earth Surface*, **112** (F2).

Perdikatsis, V. (2010). Mineralogy of the Saharan aeolian dust in Crete: Examples from the period 2004-2009 *in Bulletin of the Geological Society of Greece*, **43**(5), 2571-2576.

Pilkey, O., Neal, W., Cooper, J., and Kelley, J. (2011). *The World's Beaches: A Global Guide to the Science of the Shoreline (first edition)*, CA, USA, /University of California Press. 51-102.

Prospero, J., Ginoux, P., Torres, O., Nicholson, S., and Gill, T. (2002). Environmental Characterization of Global Sources of Atmospheric Soil Dust Identified with the Nimbus 7 Total Ozone Mapping Spectrometer (TOMS) Absorbing Aerosol Product, *Reviews of Geophysics*, **40**, 2-31.

Prospero, J., and Mayol-Bracero, O. (2013). Understanding the Transport and Impact of African Dust on the Caribbean Basin, *Bulletin of the American Meteorological Society* **94**(9), 1329-1337.

Rodriguez-Navarro, C. (2018). Mineralogy and Physicochemical Features of Saharan Dust Wet Deposited in the Iberian Peninsula During an Extreme Red Rain Event, *Atmospheric Chemistry Physics*, **18**, 10089-10122.

Sakhamuri, S., and Cummings, S. (2019). Increasing trans-Atlantic intrusion of Sahara dust: a cause for concern? *Planetary Health*, **3**, 242-242.

Saribudak, M. (2016). Near-surface Geophysical Mapping of an Upper Cretaceous submarine volcanic vent in Austin, Texas, USA, *The Leading Edge*, **35**, 986-994.

Stringer, L. (2019). SPMA Contributors to IPCC Special on Climate Change and Land, *IPCC Annex III*, 839-2966.

TPWD Playas. (n.d.). *TPWD.* Retrieved December 27, 2021, from https://tpwd.texas.gov/landwater/land/habitats/high_plains/wetlands/playa.phtml

Tabor, N., Michel, L., and Myers, T. (2017). *Sedimentologist's guide for recognition, description, and classification of paleosols in terrestrial depositional systems*, El Sevier 165-208.

Williams, R., et al. (2016). Glacial to Holocene changes in trans-Atlantic Saharan dust transport and dust climate feedbacks, *Science Advances*, 23 Nov. 2016:10.1126.

Westrich, J., Ebling, A., Landing, W., Joyner, J., Kemp, K., Griffin, D., and Lipp, E. (2016). Sahara dust nutrients promote Vibrio bloom formation in marine surface waters, *PNAS*, **113**(21), 5964-5969.

USGS Playas. (n.d.). *USGS.* Retrieved December 28, 2021, from https://pubs.usgs.gov/of/2004/1007/playas.html

XRF manual. (n.d.). Spectro. Retrieved March 15, 2021, from www.spectro.com/user-manual-spectro-xepos-xrf

APPENDICES

APPENDIX A

Location 1 - Playa

	% Clay	% Silt	% Sand	Total
Average of '1A 20cm'	16.55	54.57	28.86	99.98
Average of '1A 15cm'	19.37	60.43	20.17	99.97
Average of '1A 10cm'	19.18	54.29	26.5	99.97
Average of '1A 5cm'	23.7	56.93	19.37	100
Average of '1B 20cm'	21.39	58.6	20.01	100
Average of '1B 15cm'	26.47	61.49	12.04	100
Average of '1B 10cm'	23.82	58.78	17.44	100.04
Average of '1B 5cm'	32.9	57.42	9.69	100.01
Average of '1C 75cm'	28.39	59.96	11.6	99.95
Average of '1C 70cm'	31.5	57.54	10.97	100.01
Average of '1C 65cm'	26.37	54.68	18.96	100.01
Average of '1C 60cm'	44.53	48.91	6.56	100
Average of '1C 55cm'	14.22	27.17	58.62	100.01
Average of '1C 50cm'	28.62	52.76	18.6	99.98
Average of '1C 45cm'	29.33	55.47	15.21	100.01
Average of '1C 40cm'	28.66	43.28	28.02	99.96
Average of '1C 35cm'	37.65	55.41	6.94	100
Average of '1C 30cm'	32.84	56.78	10.39	100.01
Average of '1C 25cm'	34.18	55.81	10.01	100
Average of '1C 20cm'	33.48	48.55	17.98	100.01
Average of '1C 15cm'	34.75	53.61	11.65	100.01
Average of '1C 10cm'	39.13	52.62	8.25	100
Average of '1C 5cm'	36.63	52.89	10.48	100
Average of '1D 50cm'	20.45	48.71	30.87	100.03
Average of '1D 45cm'	30.43	52.67	16.88	99.98
Average of '1D 40cm'	23.27	52.21	24.52	100
Average of '1D 35cm'	32.18	31.67	36.11	99.96
Average of '1D 30cm'	18.83	52.98	28.18	99.99
Average of '1D 25cm'	23.02	50.34	26.6	99.96
Average of '1D 20cm'	23.99	55.46	20.55	100
Average of '1D 15cm'	19.63	57.19	23.21	100.03
Average of '1D 10cm'	23.27	52.2	24.52	99.99
Average of '1D 5cm'	35.08	64.86	0.06	100

Location 2 - Dune

	Clay %	Silt %	Sand %	Total
Average of 'l2 2a surface'	0	0.31	99.7	100.01
Average of 'l2 2a 190cm'	0	0.4	99.58	99.98
Average of 'l2 2a 185cm'	0	0.21	99.78	99.99
Average of 'l2 2a 180cm'	0	0.12	99.88	100
Average of 'l2 2a 175cm'	0	0.36	99.63	99.99
Average of 'l2 2a 170cm'	0	0.37	99.62	99.99
Average of 'l2 2a 165cm'	0	0.32	99.65	99.97
Average of 'l2 2a 160cm'	0	0.72	99.25	99.97
Average of 'l2 2a 155cm'	0	0.63	99.36	99.99
Average of 'l2 2a 150cm'	0	0.35	99.65	100
Average of 'l2 2a 145cm'	0	0.48	99.52	100
Average of 'l2 2a 140cm'	0	0.62	99.37	99.99
Average of 'l2 2a 135cm'	0	0.66	99.34	100
Average of 'l2 2a 130cm'	0	0.69	99.3	99.99
Average of 'l2 2a 125cm'	0	0.51	99.48	99.99
Average of 'l2 2a 120cm'	0	0.2	99.81	100.01
Average of 'l2 2a 115cm'	0	1.09	98.9	99.99
Average of 'l2 2a 110cm'	0	0.5	99.5	100
Average of 'l2 2a 105cm'	0	1.02	98.98	100
Average of 'l2 2a 100cm'	0	0.44	99.56	100
Average of 'l2 2a 95cm'	0	0.89	99.15	100.04
Average of 'l2 2a 90cm'	0	1.07	98.91	99.98
Average of 'l2 2a 85cm'	0	1.23	98.78	100.01
Average of 'l2 2a 80cm'	0	1.09	98.91	100
Average of 'l2 2a 75cm'	0	0.69	99.29	99.98
Average of 'l2 2a 70cm'	0	0	99.98	99.98
Average of 'l2 2a 65cm'	0	0.61	99.4	100.01
Average of 'l2 2a 60cm'	0	0.31	99.66	99.97
Average of 'l2 2a 55cm'	0	1.36	98.64	100
Average of 'l2 2a 50cm'	0	1	99	100
Average of 'l2 2a 45cm'	0	0.8	99.19	99.99
Average of 'l2 2a 40cm'	0	0.37	99.63	100
Average of 'l2 2a 35cm'	15.37	18.18	66.44	99.99
Average of 'l2 2a 30cm'	62.28	35.2	2.52	100
Average of 'l2 2a 25cm'	49.79	42.51	7.72	100.02
Average of 'l2 2a 20cm'	48.92	29.73	21.33	99.98
Average of 'l2 2a 15cm'	53.64	44.05	2.32	100.01
Average of 'l2 2a 10cm'	59.65	35.78	4.55	99.98
Average of 'l2 2a base'	64.13	35.1	0.77	100